IEEE Access
Multidisciplinary | Rapid Review | Open Access Journal

Received January 9, 2018, accepted February 9, 2018, date of publication February 19, 2018, date of current version March 15, 2018.

Digital Object Identifier 10.1109/ACCESS.2018.2807415

A High-Isolation Two-Port Planar Antenna System for Communication and Radar Applications

TANNER J. DOUGLAS, (Student Member, IEEE), AND KAMAL SARABANDI, (Fellow, IEEE)
Department of Electrical Engineering and Computer Science, University of Michigan, Ann Arbor, MI 48109 USA

Corresponding author: Tanner J. Douglas (tjdoug@umich.edu)

This work was supported by the U.S. Army Research Laboratory through collaborative participation in the Microelectronics Center of Micro Autonomous Systems and Technology Collaborative Technology Alliance under Contract W911NF-08-2-0004.

ABSTRACT This paper presents a novel approach to achieve a very high level of isolation between the two ports of a compact antenna system for communication and radar applications. Orthogonal polarization and a special symmetric arrangement of two-element arrays of transmitter and receiver antennas are used to achieve high isolation levels. Identical rectangular patch antennas are designed for operation at 6 GHz, and are arranged in a square grid configuration with 90° rotational symmetry in this design. A pair of transmitters and a pair of receivers are fed perfectly out of phase with 180° couplers. The entire system is simulated and fabricated. We measure the prototype antenna's isolation, and use the absolute gain measurement technique and standard far field antenna pattern measurement technique to characterize it's realized gain and radiation pattern. It is found that exploiting symmetry in this manner leads to isolation of 63.7 dB. This indicates that carefully designed and constructed systems could reasonably exhibit isolation on the order of 70 dB or more using this method.

INDEX TERMS Isolation, patch antennas, orthogonal polarization, two-port antenna.

I. INTRODUCTION

As mobile communication technologies continue to develop, and the demand for more, cheaper, and faster data increases, it is necessary to implement spectrum-efficient communication techniques to minimize further cluttering of the already congested radio spectrum. One way to accomplish this is by enabling communication with simultaneous transmit and receive at a single frequency [1], [2]. Since frequency division duplexing uses separate frequencies for transmitting and receiving, condensing both directions into a single frequency will effectively double the amount of data that can be communicated in a given bandwidth. Additionally, short range radars such as automotive radars make use of a continuous-wave spectrum to keep the peak transmit power low [3]–[5]. For such systems, very high isolation between transmit and receive is needed for high receiver dynamic range and small target detection. As a result, the transmit and receive antennas are usually separated to achieve better isolation.

The main challenge to overcome in order to achieve these goals is the coupling between the transmitter and receiver. If the two ports are not sufficiently isolated, the desired communication signal or radar return can easily become indistinguishable due to the radiation coupled from the transmitter to the receiver.

An obvious approach is to make use of orthogonal polarization. If the transmitter and receiver are linearly polarized and oriented orthogonal to each other, then ideally they would not interfere with each other. In reality all antennas generate cross-polarized fields, so orthogonal polarization is usually not enough to ensure the required isolation for compact designs. The concept of full-duplex was first introduced in connection with a common aperture polarimetric active radar calibrator to produce relatively small calibration targets with large radar cross-section [6]. In this design a square horn was connected to a high isolation orthomode transducer to separate the receive signal from the transmit signal. The same idea was later perfected to achieve more than 80 dB isolation between the two ports [7].

In this paper, we investigate the use of a special symmetry to achieve high isolation between orthogonally

polarized patch antennas. This will allow for implementation of a compact, two-port, planar antenna system with very high isolation. Rectangular patch antennas are well suited to this technique for several reasons. In addition to being linearly polarized, their bandwidth can be increased by including U-shaped slots in the patch [8]–[10]. We arrange two transmitting patch elements and two receiving patch elements in a square grid with ninety-degree rotational symmetry about the center. In this configuration, the coupling between transmitter-receiver pairs are shown to be equal. Thus by exciting the transmitters perfectly out of phase and subtracting the two receiver signals, we can achieve very high levels of cancellation despite close proximity between the radiating elements. A feed network featuring a pair of one-hundred-eighty-degree hybrid couplers is designed to perform the out-of-phase excitation and signal subtraction. Full-wave electromagnetic analysis in HFSS is then used to simulate the entire system. Finally, we construct a prototype of the device and compare its measured performance to that of the simulation.

This antenna system has potential applications across several disciplines. One major application is in full-duplex communication systems. Assuming a maximum power output of 40dBm, an additional isolation of about 30dB that can be achieved at the IF band, and the fact that signal processing algorithms are capable of attenuating known transmit signals at baseband by 30dB, 80dB of RF isolation can reduce the transmitter leakage to about −90dBm or less. This will be sufficient for most practical cases to detect the desired received signals with a relatively high signal to interference ratio. Additionally, the antenna system could be utilized in high-cross-section active radar calibration targets.

The design presented here has a relatively narrow band of operation centered at 6 GHz for demonstration of the concept. The surrounding frequency band from roughly 5 GHz to 7 GHz is licensed by the FCC for applications in mobile communications, fixed-satellite service, radio-location, and radionavigation. It also includes the 5.8 GHz ISM band. With some minor scaling, the antenna system could be adjusted to shift the operation frequency to meet the needs of applications in any of these areas. Furthermore, the bandwidth can be enhanced by using different radiating elements and a modified feed network, allowing for operation over a much larger portion of the C band.

II. THEORY

Fig. 1 shows the configuration of a compact two-port antenna system intended to provide very high isolation (>60dB). This antenna system functions by exploiting the ninety-degree rotational symmetry of a square grid. The operating principle behind this design is the near equality of the transmission coefficients between any pair of transmitter patch and receiver patch. In order to illustrate this mathematically, it is most useful to consider the scattering parameters of a four-port network, with each port corresponding to one of the four patch elements.

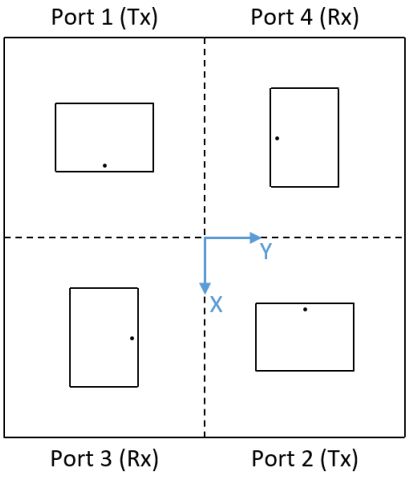

FIGURE 1. Geometry of the square grid configuration of the two transmitter patch elements and two receiver patch elements. A coordinate system is also defined.

The scattering parameters for an N-port network are defined as follows:

$$\begin{bmatrix} V_1^- \\ V_2^- \\ \vdots \\ V_N^- \end{bmatrix} = \begin{bmatrix} S_{11} & S_{12} & \cdots & S_{1N} \\ S_{21} & S_{22} & \cdots & S_{2N} \\ \vdots & \vdots & \ddots & \vdots \\ S_{N1} & S_{N2} & \cdots & S_{NN} \end{bmatrix} \begin{bmatrix} V_1^+ \\ V_2^+ \\ \vdots \\ V_N^+ \end{bmatrix} \quad (1)$$

where V_m^- are the reflected voltage waves, V_n^+ are the incident voltage waves, and S_{mn} are the scattering parameters [11].

Suppose the transmitters are assigned port labels 1 and 2, and the receivers are assigned port labels 3 and 4. Due to the ninety-degree rotational symmetry of the geometry, all elements of the diagonal of the scattering matrix are equal. Furthermore, the rotational symmetry in combination with the reciprocity theorem dictate that the coupling between either transmitter element and either receiver element will be equal, and the coupling between the two transmitters is equal to the coupling between the two receivers. Therefore, the scattering matrix can be simplified as follows:

$$\begin{bmatrix} S_{11} & S_{12} & S_{13} & S_{14} \\ S_{21} & S_{22} & S_{23} & S_{24} \\ S_{31} & S_{32} & S_{33} & S_{34} \\ S_{41} & S_{42} & S_{43} & S_{44} \end{bmatrix} = \begin{bmatrix} S_1 & S_2 & S_3 & S_3 \\ S_2 & S_1 & S_3 & S_3 \\ S_3 & S_3 & S_1 & S_2 \\ S_3 & S_3 & S_2 & S_1 \end{bmatrix}. \quad (2)$$

Suppose that we excite the transmitters with equal magnitude and opposite phase, and that there exist impedance mismatches at the receiver ports. Then the following relations can be made:

$$\begin{aligned} V_2^+ &= -V_1^+ \\ V_3^+ &= \Gamma_3 V_3^- \\ V_4^+ &= \Gamma_4 V_4^-, \end{aligned} \quad (3)$$

where Γ_3 and Γ_4 are reflection coefficients due to the receiver port mismatch. These reflection coefficients are defined looking out of ports 3 and 4 and looking into the respective

loads, and arise if the loads are not matched to the system impedance. Substituting (2) and (3) into the third and fourth rows of (1), we obtain:

$$V_3^- = S_3V_1^+ - S_3V_1^+ + S_1\Gamma_3V_3^- + S_2\Gamma_4V_4^-$$
$$V_4^- = S_3V_1^+ - S_3V_1^+ + S_2\Gamma_3V_3^- + S_1\Gamma_4V_4^-. \quad (4)$$

The first two terms of the right hand side of each equation above cancel, and it can easily be shown that the solution of (4) is $V_3^- = V_4^- = 0$, unless $(1 - S_1\Gamma_3)(1 - S_1\Gamma_4) = S_2^2\Gamma_3\Gamma_4$. However, this condition cannot be the case in general, since there is no deterministic relationship between the scattering parameters and reflection coefficients. Furthermore, we expect the scattering parameters and reflection coefficients to be close to zero, in which case this condition is clearly false, as the left hand side is approximately one and the right hand side is approximately zero. Thus under these conditions, the coupling from the transmitters to the receivers is entirely canceled. Note that while the transmitters are excited out of phase, they are also oriented in the opposite direction. Therefore, the main lobe of the beam still points in the desired boresight direction.

To ensure that the receiver beam also points in this direction, we must subtract the signals at the two receiver ports. For the purpose of simulating the isolation of this configuration, we assume the receivers are presented with matched loads ($\Gamma_3 = \Gamma_4 = 0$). With this assumption, and the relations in (3), we can subtract the fourth row from the third row of (1) to obtain:

$$V_3^- - V_4^- = (S_{31} - S_{32} - S_{41} + S_{42})V_1^+. \quad (5)$$

Therefore, we can measure the isolation as $S_{31} - S_{32} - S_{41} + S_{42}$. From (2), we expect each of these parameters to be equal to each other. Thus we expect nearly perfect isolation.

III. ANTENNA DESIGN

A rectangular patch antenna is designed to operate at 6 GHz. The patch is excited by a coaxial probe fed from behind the ground plane through the substrate [12]. The substrate has a dielectric constant of $\varepsilon_r = 2.2$ and a height of h = 3.175 mm (0.125 in.). The geometry of the patch is shown in Fig. 2, while the design parameters are tabulated in Table 1. Note that at this stage the geometric center of the patch coincides with the geometric center of the substrate. The antenna is well matched, presenting a simulated input reflection coefficient below −70 dB at the design frequency, as shown in Fig. 3. It is linearly polarized and provides a realized gain of more than 8.4 dB.

Next, four of these patch antennas are arranged according to the square grid configuration shown in Fig. 1. Initially the patches are positioned such that their geometric centers align with the geometric centers of their respective quadrants of the substrate. However, since the radiation pattern is now influenced by array effects, the distance from the patch center to the array center is allowed to vary, as depicted in Fig. 4. Thus initially the value of the dimension D_c is 25.40 mm

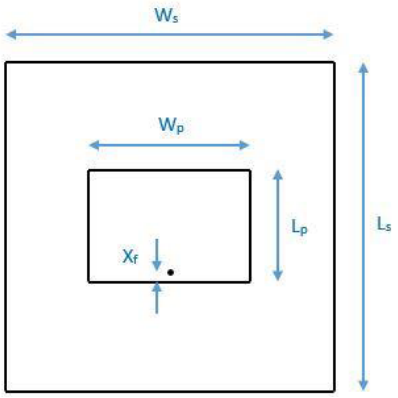

FIGURE 2. Geometry of the patch antenna, showing the dimensions of the substrate and patch.

TABLE 1. Design parameters of patch antenna.

Symbol	Dimension	Length (mm)	Length (in.)
L_s	substrate length	50.80	2.000
W_s	substrate width	50.80	2.000
L_p	patch length	15.14	0.596
W_p	patch width	20.35	0.801
X_f	feed-to-edge distance	0.711	0.028

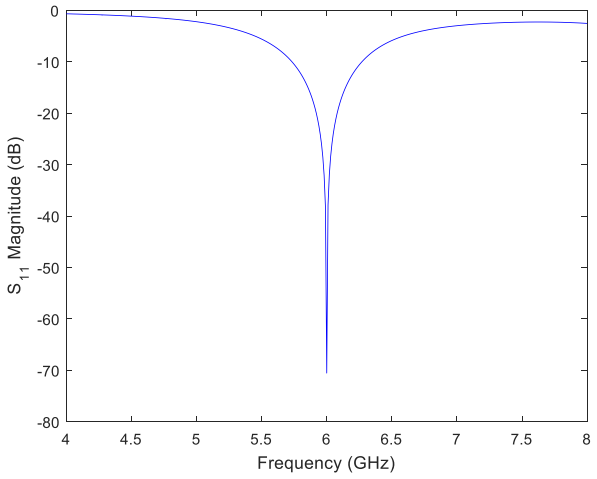

FIGURE 3. The simulated input reflection coefficient of the patch antenna is shown.

(1.000 in.). This parameter is optimized to maximize the total boresight gain when both transmitter patches are simultaneously excited out of phase, as shown in Fig. 5. the value D_c = 16.51 mm (0.650 in.) is chosen. Therefore the centers of the patch elements are only 33.02 mm (1.300 in.) apart, which is less than a free-space wavelength at 6 GHz.

At this stage of the design, the array is treated as a four-port network and simulated to measure the isolation between the transmitter pair and receiver pair according to (5). The result is shown in Fig. 6. At the design frequency of 6 GHz, an isolation of more than 90 dB is achieved. Over the band from 4.5 GHz to 7.5 GHz, the isolation is greater than 75 dB.

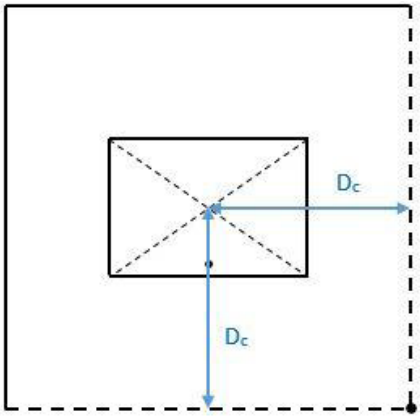

FIGURE 4. The distance between the center of the patch and the edge of its quadrant (D_c) is allowed to vary.

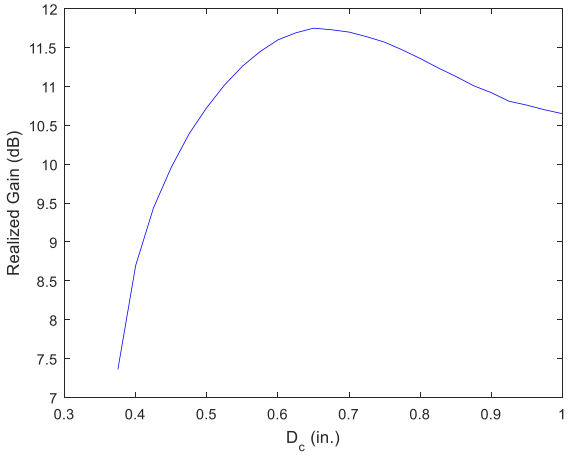

FIGURE 5. The total realized gain at boresight is plotted for varying D_c, when ports 1 and 2 are simultaneously excited out of phase. A maximum is observed at 0.650 in.

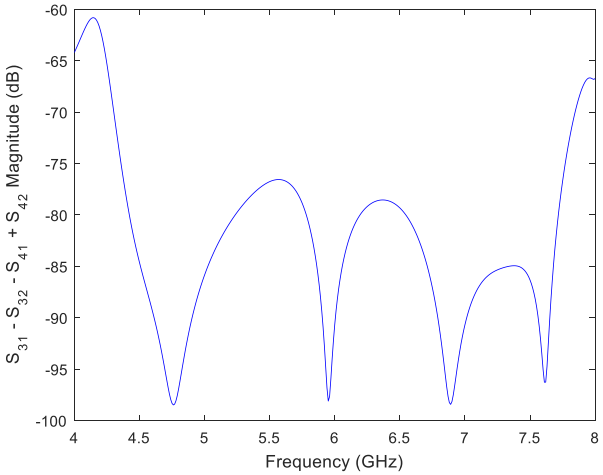

FIGURE 6. The quantity plotted on the vertical axis is a measure of the total coupling from the transmitters (ports 1 and 2) to the receivers (ports 3 and 4) when the transmitters are excited perfectly out of phase and the received signals are subtracted, as derived in (5). The isolation at 6 GHz is shown to be greater than 90 dB.

Perfect isolation is not achieved due to numerical round-off error and non-identical meshes for the four antennas. Basically, the automatic meshing does not preserve the geometrical symmetry exactly.

The final step in the design process was to design a feed network for the array of patches. The feed network consists of two one-hundred-eighty-degree hybrid couplers, microstrip traces to connect to the patch probes, and resistor pads to terminate the isolated ports of the couplers. This network shares a ground plane with the patches, and has a substrate with $\varepsilon_r = 2.2$ and height $h = 0.127$ mm (0.005 in.). The very thin substrate helps to minimize unwanted coupling between the traces.

With the transmitters and receivers now connected via the couplers, the antenna is now treated as a two-port network with the transmit port assigned label 1 and the receive port assigned label 2 (note that the choice of transmit versus receive is arbitrary). Isolation can therefore be measured directly by observing the S_{21} scattering parameter. Some minor adjustments were made to the patch dimensions at this stage to attempt to increase the isolation and return loss, and the final design parameters are reported in Table 2. The simulated isolation at 6 GHz is 66.2 dB.

TABLE 2. Final design parameters of patch antenna.

Symbol	Dimension	Length (mm)	Length (in.)
L_s	substrate length	50.80	2.000
W_s	substrate width	50.80	2.000
L_p	patch length	14.94	0.588
W_p	patch width	19.91	0.784
X_f	feed-to-edge distance	0.635	0.025
D_c	center-to-edge distance	16.51	0.650

IV. FABRICATION AND MEASUREMENT

A prototype antenna was fabricated using the design described above. The substrate material is Roger RT/duroid 5880 ($\varepsilon_r = 2.2$, $\tan\delta = 0.0009$ at 10 GHz). Fig. 7 shows photographs of the antenna.

The transmitter and receiver return loss and isolation were measured using a vector network analyzer. The antenna was placed in an anechoic chamber during the measurement to minimize coupling due to reflections from nearby objects.

The gain of both the transmitter and receiver were measured using the absolute gain measurement technique [13], while the radiation patterns were measured using the standard far field antenna pattern measurement technique. The measurement setup is depicted in Fig. 8.

Due to the shape of the array, the radiation pattern is the broadest and narrowest at forty-five-degree angles from the E- and H- planes of the individual patches. Therefore, in addition to measuring the patterns in the E- and H- planes ($\phi = 0°$ and $\phi = 90°$), we also measure the patterns in the $\phi = 45°$ and $\phi = 135°$ planes. Additionally, the cross-polarized gain is measured by orienting the prototype antenna such that its polarization is orthogonal to that of the ancillary antenna, and comparing the received power to the case with the polarizations aligned.

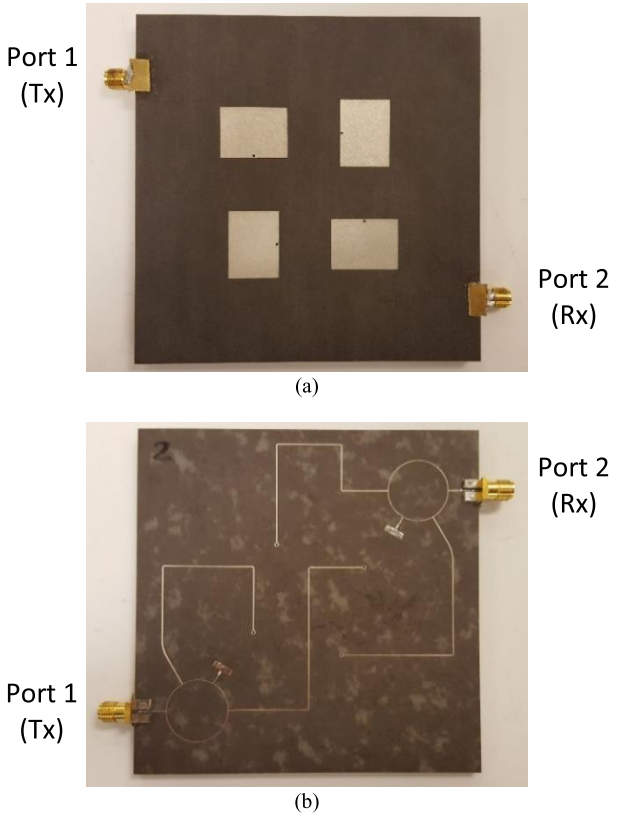

FIGURE 7. Photographs of the prototype antenna: (a) top view showing the square grid array of patches; (b) bottom view showing the feed network.

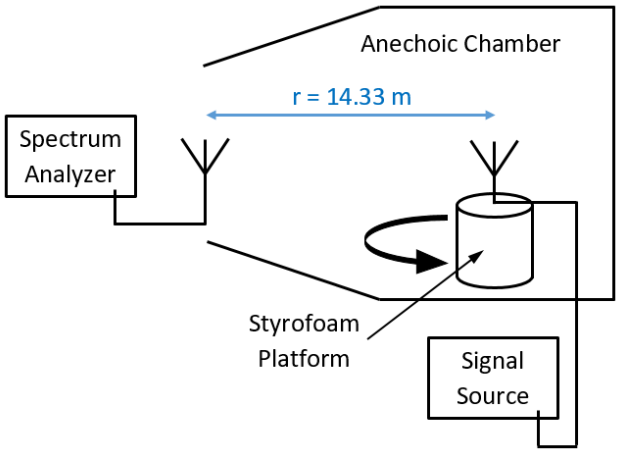

FIGURE 8. Setup for absolute gain measurement technique and standard far field antenna pattern measurement technique. For the gain measurement, three antennas are permuted in the two positions. For the pattern measurement the prototype antenna is rotated atop the Styrofoam platform.

V. RESULTS

The measured scattering parameters of the antenna are shown in comparison to the simulation results in Fig. 9. Table 3 summarizes the measured and simulated return loss and isolation at the design frequency of 6 GHz.

Fig. 10 and Fig. 11 show the measured and simulated realized gain patterns for the transmitter and receiver,

TABLE 3. Antenna return loss and isolation performance at 6 GHz.

	Simulation	Measurement
Port 1 Return Loss	49.9 dB	22.1 dB
Port 2 Return Loss	30.8 dB	31.7 dB
Isolation	66.2 dB	63.7 dB

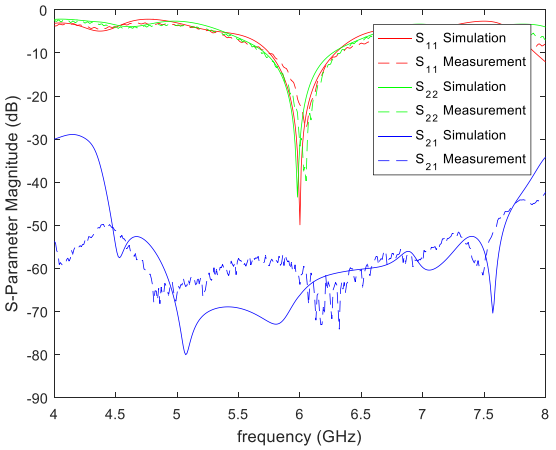

FIGURE 9. Simulated and measured scattering parameters of the antenna, showing the return loss and isolation.

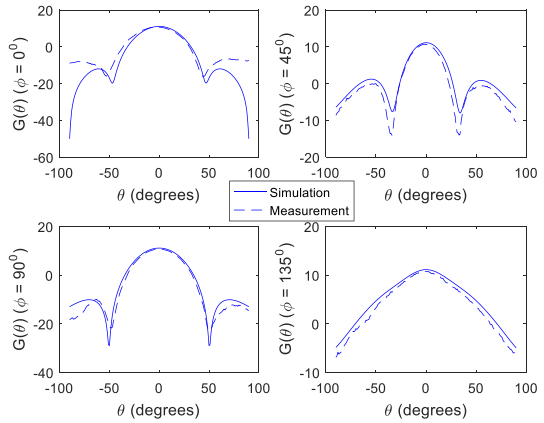

FIGURE 10. Port 1 (transmitter) simulated and measured antenna radiation pattern at 6 GHz: (top left) measured along the E-plane; (top right) measured along the narrow cross-section of the pattern; (bottom left) measured along the H-plane; (bottom right) measured along the broad cross-section of the pattern.

respectively, both in the E- and H- planes, and for angles $\phi = 45°$ and $\phi = 135°$. These angles correspond to the broadest and narrowest cross-sections of the radiation patterns. Fig. 12 shows the cross-polarized patterns in the E- and H- planes. The features of the radiation pattern are presented in Table 4.

VI. DISCUSSION

Although theoretically the symmetric array configuration used in this design should exhibit complete cancellation of coupled fields between the patch elements, and although simulations of the array without including the feed network indicated isolation potentially as high as 90 dB, the addition of the feed network reduces the simulated isolation to only

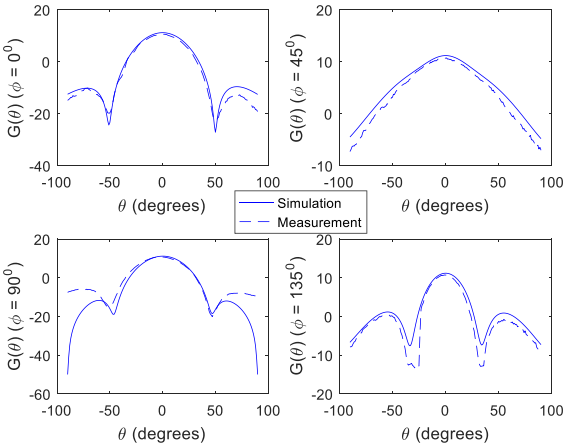

FIGURE 11. Port 2 (receiver) simulated and measured antenna radiation pattern at 6 GHz: (top left) measured along the H-plane; (top right) measured along the broad cross-section of the pattern; (bottom left) measured along the E-plane; (bottom right) measured along the narrow cross-section of the pattern.

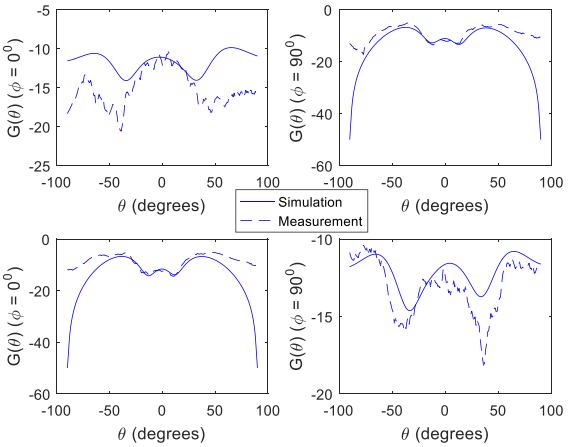

FIGURE 12. Simulated and measured cross-polarized radiation pattern at 6 GHz: (top left) measured along the E-plane of port 1; (top right) measured along the H-plane of port 1; (bottom left) measured along the H-plane of port 2; (bottom right) measured along the E-plane of port 2.

TABLE 4. Antenna radiation pattern features at 6 GHz.

	Simulation	Measurement
Port 1:		
Peak Realized Gain	11.1 dB	10.7 dB
Cross-Pol. Gain (θ = 0°)	-11.1 dB	-12.1 dB
-3dB Angles, Narrow Direction	-15°, +15°	-15°, +13°
-3dB Beamwidth, Narrow Direction	30°	28°
Null Angles, Narrow Direction	-34°, +34°	-34°, +33°
Side-lobe Angles, Narrow Direction	-55°, +55°	-57°, +56°
Side-lobe level, Narrow Direction	-9.9 dB, -10.2 dB	-10.7 dB, -11.3 dB
-3dB Angles, Broad Direction	-29°, +29°	-27°, +26°
-3dB Beamwidth, Broad Direction	58°	53°
Port 2:		
Peak Realized Gain	11.2 dB	10.6 dB
Cross-Pol. Gain (θ = 0°)	-11.6 dB	-12.4 dB
-3dB Angles, Narrow Direction	-15°, +15°	-15°, 14°
-3dB Beamwidth, Narrow Direction	30°	29°
Null Angles, Narrow Direction	-34°, +34°	-29°, +33°
Side-lobe Angles, Narrow Direction	-55°, +55°	-55°, +55°
Side-lobe level, Narrow Direction	-10.1 dB, -10.3 dB	-10.2 dB, -11.4 dB
-3dB Angles, Broad Direction	-29°, +29°	-29°, +26°
-3dB Beamwidth, Broad Direction	58°	55°

66.2 dB. A major contributing factor to this significant drop-off is the coupling between the mictrostrip traces within the feed network. For this reason, it is important to minimize the thickness of the feed network substrate in order to confine the fields closely around the copper traces. It is possible that using other transmission line architectures, such as stripline or grounded coplanar waveguide could provide better performance. However, such transmission lines are more complicated to implement and here we used microstrip transmission lines to demonstrate the concept. We recognize that our current feed network limits the isolation we are able to attain, and plan to design improved versions for future work. Additionally, we have found that there is a correlation between the simulated isolation and the fineness of the mesh used in the substrates and copper traces. Often the isolation can be improved in simulation by using a finer mesh, but at the cost of speed.

The performance of the prototype matches the simulated performance reasonably closely, both in terms of the scattering parameters and in terms of the radiation pattern. The measured isolation of 63.7 dB falls just short of the simulated value. The measured radiation pattern aligns very closely with the simulation, the major differences including a slight angular shift, a difference of around 1–2 dB on average over the angular sweep between the measured pattern and simulated pattern, and sharper nulls in the measured pattern along the narrow cross-section compared to the simulated pattern. The angular shift could be attributed to misalignment of the antenna boresights by around a degree during the setup for the measurement. The lower realized gain is likely due to losses in the system that were not accounted for in simulation, such as connector insertion loss and protective tin plating on the copper conductors. Additionally, the absolute gain measurement assumes that the antennas are separated by free space, which is not truly the case in an anechoic chamber, and this could lead to additional uncertainty in the measured gain. The sharp measured nulls may be a reflection of the fact that the total gain in the vicinity of the nulls receives a boost due to the presence of cross polarized fields, which are not received as strongly by the linearly polarized ancillary antenna.

While 63.7 dB is a relatively high isolation between transmit and receive ports in such close proximity, this does

fall short of the isolation that we are targeting to implement a communication system with simultaneous transmit and receive. However, we have noticed several phenomena indicating that higher isolation levels should be possible. Although the antenna's isolation was measured in the anechoic chamber in order to reduce the impact of reflections from the environment, we still observe very rapid fluctuations in the isolation response, which indicates that reflections are not entirely eliminated. By positioning an additional foam absorber in front of the antenna boresight, we have found that the isolation can be improved slightly. Additionally, experimenting with the RF cables attached to the antenna system during the measurement has indicated that the isolation is sensitive to the position of these cables, since they perturb the ninety-degree rotational symmetry. Depending on the particular arrangement of the RF cables and the position of the foam absorber, we measure a range of isolation from anywhere in the 60s of dB to more than 70 dB. The reported value of 63.7 dB corresponds to a typical result that is repeatable by simply making the measurement in the anechoic chamber with a direct cable connection and no additional absorber. In practice the transmitter and receiver circuitry are embedded in the backplane of the antenna system and are thus invisible to the radiating and receiving antennas. We do believe that the ninety-degree rotational symmetry used in this design is capable of achieving isolation levels of more than 70 dB and possibly more than 80 dB in the absence of the connectors and the RF cables used for the S_{21} measurement, especially with further optimization of the feed network.

VII. WIDEBAND DESIGN

Additionally, our goal is to implement this concept not only for single frequency designs, but for wideband applications as well. One of the challenges associated with this is the need for a one-hundred-eighty-degree hybrid coupler that functions over a large bandwidth to feed the transmitters perfectly out of phase and subtract the received signals. Since this will be difficult to achieve over a wide bandwidth, we look at the effect of allowing a small deviation from perfect out-of-phase excitation and subtraction. Suppose we have the following:

$$\begin{aligned} V_2^+ &= -V_1^+ e^{j\Delta\phi_T} \\ V_R &= V_3^- - V_4^- e^{j\Delta\phi_R}, \end{aligned} \tag{6}$$

where $\Delta\phi_T$ and $\Delta\phi_R$ are the phase variations from one hundred and eighty degrees of the phase differences between the transmitter signals and receiver signals, respectively, and V_R is the total wave coupled to the receivers from the transmitters. Substituting (6) and (2) into (1), and allowing for impedance mismatch as in the second and third equations of (3), we can solve for V_R as follows:

$$\begin{aligned} V_R = V_1^+ &\frac{S_3(1-e^{j\Delta\phi_T})}{(1-S_1\Gamma_3)(1-S_1\Gamma_4)-S_2^2\Gamma_3\Gamma_4} \\ &\times((1-S_1\Gamma_4+S_2\Gamma_4)-(1-S_1\Gamma_3+S_2\Gamma_3)\,e^{j\Delta\phi_R}). \end{aligned} \tag{7}$$

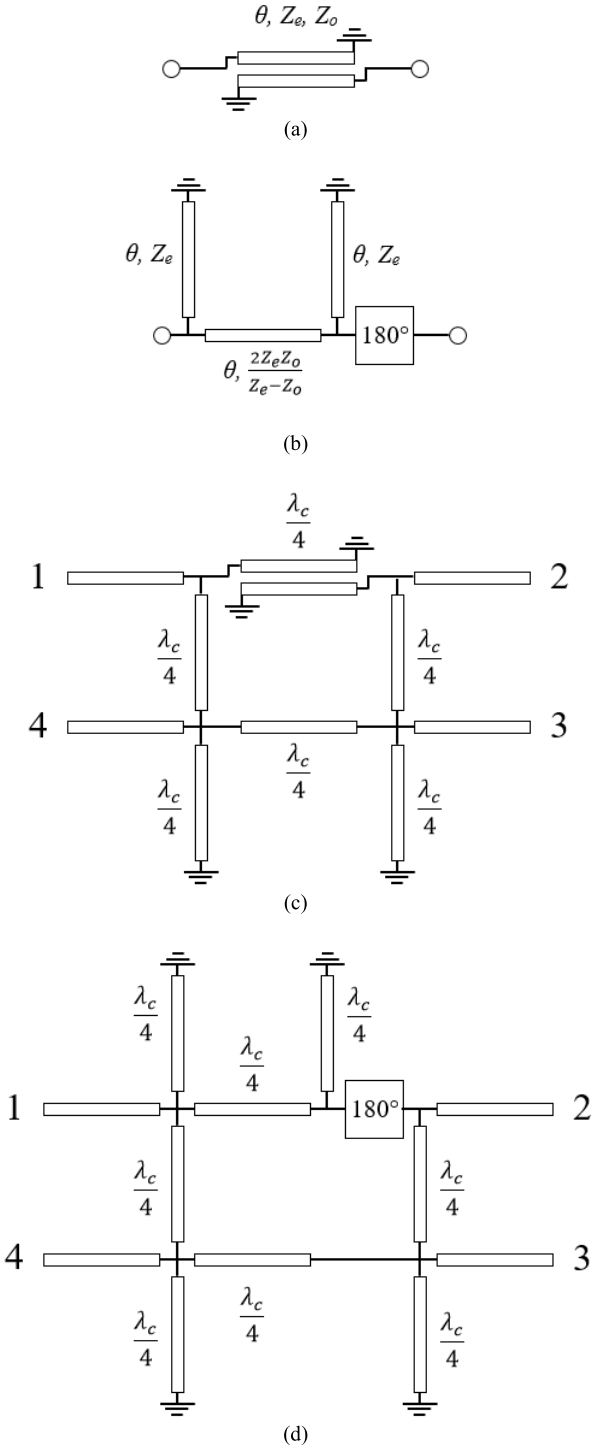

FIGURE 13. The coupled line section with opposite ends of each line shorted in (a) can be modeled by the equivalent circuit in (b). Inserting (a) in place of the 3λ/4 line of the rat-race coupler, as shown in (c), produces the equivalent circuit shown in (d). The extra shorted quarter wave lines are required to maintain the symmetry of the design. λ_c is the wavelength at the center frequency of the design band, and the 180° block represents an ideal phase inverter.

Based on our estimates of the scattering parameters S_1, S_2, and S_3, and the reflection coefficients Γ_3 and Γ_4, (7) indicates that the received coupling from the transmitters can be kept

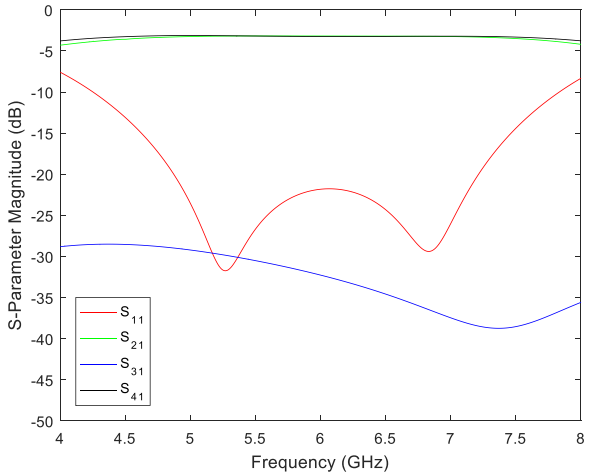

FIGURE 14. The simulated scattering parameters of the wideband coupler are shown.

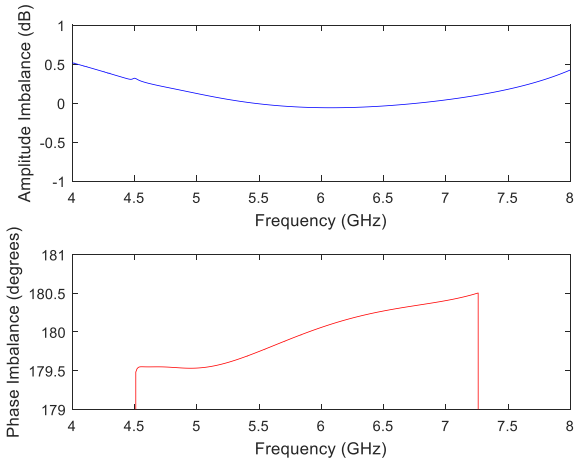

FIGURE 15. The amplitude imbalance (top) and phase imbalance (bottom) between S_{41} and S_{21} of the wideband coupler are shown.

below −80 dB if $\Delta\phi_T$ and $\Delta\phi_R$ are within about ±3° from zero. This result indicates that a wideband hybrid coupler with low phase imbalance will be required to implement a system using this symmetric configuration over a wide bandwidth.

To design a coupler capable of providing a 3 dB power split with a one-hundred-eighty-degree phase difference over a bandwidth of about 25%, we begin by considering a microstrip rat race coupler, a standard coupler for out-of-phase power division. However, due to the presence of the transmission line of length 3λ/4 in the rat race, the perfect phase difference between the outputs is not held when the frequency drifts from the center frequency. To address this issue, we replace the 3λ/4 line with a coupled line section of length λ/4 with one end of each line shorted, as in [14] and [15]. This configuration behaves like a quarter-wave transmission line in series with an ideal phase inverter, as shown in Fig. 13. Using this substitution provides a constant phase difference between the two coupler outputs (ports 2 and 4 when port 1 is used as the input) as frequency changes, since the two paths between ports 1 and 2 have the same physical length as the two paths between ports 1 and 4. This allows for the design of a wideband one-hundred-eighty-degree coupler. Because of the two shorted quarter-wave lines in the equivalent circuit for the coupled line section, additional shorted quarter-wave lines must be placed near ports 3 and 4 to maintain the symmetry of the coupler.

Using this method to design a modified rat race coupler, we are able to achieve an equal power split with less than 0.06 dB of amplitude imbalance and less than ±0.5° of phase imbalance over the 5.24 GHz – 6.94 GHz band (about 28% bandwidth). The simulated scattering parameters of the coupler are shown in Fig. 14, while Fig. 15 shows the amplitude imbalance and phase imbalance.

The patch elements used in the current design are matched only in a narrow frequency band centered at 6 GHz. In order to present the wideband coupler with a well-matched load over its operating band, new radiating elements must be designed. The U-slot patch is capable of bandwidth on the order of 25% - 30%, and should be suitable for this purpose. Implementation of wideband U-slot patch elements and utilizing them in conjunction with the wideband coupler to design a wideband two-port antenna system with high isolation is the subject of future investigation.

VIII. CONCLUSION

In this paper it is shown that using polarization orthogonality and a novel rotational symmetry cancellation, it is possible to design a compact transmitter and receiver antenna system that has very high isolation between the two ports. By using a square grid array with ninety-degree rotational symmetry and one-hundred-eighty-degree hybrid couplers, we were able to construct a prototype antenna that matched simulation results well and exhibited isolation of 63.7 dB at the design frequency. This is quite an impressive level of isolation for an antenna system without the aid of any analog or digital cancellation, especially considering that the patches are spaced less than a wavelength apart. These results are promising, since we believe isolation levels of more than 70 dB and perhaps more than 80 dB are possible with additional design efforts. This puts us at isolation levels that would be usable in a full-duplex system with a very high receiver dynamic range.

Additionally, we have designed a one-hundred-eighty-degree hybrid coupler with low amplitude and phase imbalance over a bandwidth of 28%, which we hope to utilize in future designs to implement a wideband antenna system for communication and radar applications that require more bandwidth.

REFERENCES

[1] J. I. Choi, M. Jain, K. Srinivasan, P. Levis, and S. Katti, "Achieving single channel, full duplex wireless communication," in *Proc. ACM MobiCom*, 2010, pp. 1–12.

[2] M. Duarte and A. Sabharwal, "Full-duplex wireless communications using off-the-shelf radios: Feasibility and first results," in *Proc. Asilomar Conf. Signals, Syst., Comput.*, 2010, pp. 1558–1562.

[3] M. W. Whitt, F. T. Ulaby, and K. Sarabandi, "Polarimetric scatterometer systems and measurements," in *Radar Polarimetry for Geoscience Applications*, F. T. Ulaby and C. Elachi, Eds. Dedham, MA, USA: Artech House, 1990.
[4] D. Richardson, "An FMCW radar sensor for collision avoidance," in *Proc. Conf. Intell. Transp. Syst.*, Nov. 1997, pp. 427–432.
[5] A. Melzer, F. Starzer, H. Jager, and M. Huemer, "Real-time mitigation of short-range leakage in automotive FMCW radar transceivers," *IEEE Trans. Circuits Syst. II, Exp. Briefs*, vol. 64, no. 7, pp. 847–851, Jul. 2017.
[6] K. Sarabandi, Y. Oh, and F. T. Ulaby, "Performance characterization of polarimetric active radar calibrators and a new single antenna design," *IEEE Trans. Antennas Propag.*, vol. 40, no. 10, pp. 1147–1154, Oct. 1992.
[7] K. Sarabandi, M. Kashanianfard, A. Y. Nashashibi, L. E. Pierce, and R. Hampton, "A polarimetric active transponder with extremely large RCS for absolute radiometric calibration of SMAP radar," *IEEE Trans. Geosci. Remote Sens.*, to be published.
[8] J. Howell, "Microstrip antennas," *IEEE Trans. Antennas Propag.*, vol. AP-23, no. 1, pp. 90–93, Jan. 1975.
[9] K. F. Lee, S. L. S. Yang, A. A. Kishk, and K. M. Luk, "The versatile U-slot patch antenna," *IEEE Antennas Propag. Mag.*, vol. 52, no. 1, pp. 71–88, Feb. 2010.
[10] K. Sarabandi, A. M. Buerkle, and H. Mosallaei, "Compact wideband UHF patch antenna on a reactive impedance substrate," *IEEE Antennas Wireless Propag. Lett.*, vol. 5, no. 1, pp. 503–506, Dec. 2006.
[11] D. M. Pozar, "Microwave network analysis," in *Microwave Engineering*, 4th ed. Hoboken, NJ, USA: Wiley, 2012, ch. 4, sec. 3, pp. 178–188.
[12] K. F. Tong, K. M. Luk, and K. F. Lee, "Design of a broadband U-slot patch antenna on a microwave substrate," in *Proc. Asia–Pacific Microw. Conf.*, 1997, pp. 221–224.
[13] G. H. Bryant, "Antenna measurements," in *Principles of Microwave Measurements*. Stevenage, U.K.: Peregrinus, 1993, ch. 12, sec. 5, pp. 278–281.
[14] K. S. Ang, Y. C. Leong, and C. H. Lee, "Impedance-transforming, coupled-line 180° hybrid rings with frequency independent characteristics," in *IEEE MTT-S Int. Microw. Symp. Dig.*, vol. 3. Jun. 2003, pp. 1239–1242.
[15] S. Gruszczynski and K. Wincza, "Broadband rat-race couplers with coupled-line section and impedance transformers," *IEEE Microw. Wireless Compon. Lett.*, vol. 22, no. 1, pp. 22–24, Jan. 2012.

TANNER J. DOUGLAS received the B.S. degree in electrical and computer engineering from Carnegie Mellon University, Pittsburgh, PA, USA, in 2016. He is currently pursuing the Ph.D. degree with the Radiation Laboratory, Department of Electrical Engineering and Computer Science, University of Michigan, Ann Arbor, MI, USA.

KAMAL SARABANDI (S'87–M'90–SM'92–F'00) received the B.S. degree in electrical engineering from the Sharif University of Technology, Tehran, Iran, in 1980, the M.S. degrees in electrical engineering and in mathematics and the Ph.D. degree in electrical engineering from the University of Michigan, Ann Arbor, in 1986 and 1989, respectively.

He is currently the Director of the Radiation Laboratory and the Rufus S. Teesdale endowed Professor of Engineering with the Department of Electrical Engineering and Computer Science, University of Michigan. His research areas of interest include microwave and millimeter-wave radar remote sensing, metamaterials, electromagnetic wave propagation, and antenna miniaturization. He possesses over 30 years of experience with wave propagation in random media, communication channel modeling, microwave sensors, and radar systems and leads a large research group including two research scientists and 16 Ph.D. students. He has graduated 48 Ph.D. and supervised numerous post-doctoral students. He has served as the Principal Investigator on many projects sponsored by the National Aeronautics and Space Administration, Jet Propulsion Laboratory, Army Research Office, Office of Naval Research, Army Research Laboratory, National Science Foundation, Defense Advanced Research Projects Agency, and a large number of industries. He is currently leading the Center for Microelectronics and Sensors funded in 2008 by the Army Research Laboratory under the Micro-Autonomous Systems and Technology Collaborative Technology Alliance Program. He is also leading a newly established center in microwave sensor technology funded by King Abdulaziz City for Science and Technology.

He has published many book chapters and over 260 papers in refereed journals on miniaturized and on-chip antennas, meta-materials, electromagnetic scattering, wireless channel modeling, random media modeling, microwave measurement techniques, radar calibration, inverse scattering problems, and microwave sensors. He has also had over 630 papers and invited presentations in many national and international conferences and symposia on similar subjects.

Dr. Sarabandi served as a member of the NASA Advisory Council appointed by the NASA Administrator for two consecutive terms from 2006 to 2010. He served as the President of the IEEE Geoscience and Remote Sensing Society (GRSS) in 2015 and 2016. He is a member of Commissions F and B of URSI and is also serving as the vice Chair of the USNC URSI Commission F. He was the recipient of the Henry Russel Award from the Regent of the University of Michigan in 1997. In 1999, he received a GAAC Distinguished Lecturer Award from the German Federal Ministry for Education, Science, and Technology. He was also a recipient of the 1996 EECS Department Teaching Excellence Award and the 2004 College of Engineering Research Excellence Award. In 2005, he received the IEEE GRSS Distinguished Achievement Award and the University of Michigan Faculty Recognition Award. He was a recipient of the Best Paper Award at the 2006 Army Science Conference. In 2008, he was awarded a Humboldt Research Award from The Alexander von Humboldt Foundation of Germany and received the Best Paper Award at the IEEE Geoscience and Remote Sensing Symposium. He also received the 2010 Distinguished Faculty Achievement Award from the University of Michigan. The IEEE Board of Directors announced him as the recipient of the 2011 IEEE Judith A. Resnik Award. He was recognized by the IEEE GRSS with its 2013 Education Award and the 2017 Interactive Symposium Paper Award. In 2016, he received the Stephen S. Attwood Award from the College of Engineering, University of Michigan, a Distinguished Alumni Award from the Sharif University of Technology, and selected as a Fellow of the American Association for the Advancement of Science. In the past several years, joint papers presented by his students at a number of international symposia including, the IEEE APS'95,'97,'00,'01,'03,'05,'06,'07;'16 IEEE IGARSS'99,'02,'07;'11,'14, IEEE IMS'01, USNC URSI'04,'05,'06,'10,'11, AMTA '06, URSI GA '08,'14; and Eastern Snow Conference '16 and have received the best paper awards. He was a member of the Editorial Board of the proceedings of the IEEE and an Associate Editor for the IEEE TRANSACTIONS ON ANTENNAS AND PROPAGATION and the IEEE SENSORS JOURNAL.